The use of resonant scattering to identify stone fracture in shock wave lithotripsy

Neil R. Owen, Michael R. Bailey, and Lawrence A. Crum
Center for Industrial and Medical Ultrasound, Applied Physics Laboratory, University of Washington, 1013 NE 40th Street, Seattle, Washington 98105
nowen@apl.washington.edu; bailey@apl.washington.edu; lac@apl.washington.edu

Oleg A. Sapozhnikov and Leonid A. Trusov
Department of Acoustics, Faculty of Physics, M.V. Lomonosov Moscow State University, Leninskie Gory, Moscow 119992, Russia
oleg@acs366.phys.msu.ru; leotrusov@gmail.com

Abstract: There is currently little feedback as to whether kidney stones have fractured during shock wave lithotripsy. Resonant scattering of the lithotripter shock wave was used here to differentiate intact and fractured stone models in water. Scattering, including reflection and radiation due to reverberation from within the stone, was calculated numerically with linear elasticity theory and agreed well with measurements made with a focused receiver. Identification of fracture was possible through frequency analysis, where scatter from fractured stones was characterized by higher energy in distinct bands. High-speed photography concurrent with measurement indicated the effect was not due to cavitation.

PACS numbers: 43.20.Fn, 43.20.Gp, 43.80.Gx, 43.25.Vt [ANN]
Date Received: August 9, 2006 **Date Accepted:** October 2, 2006

1. Introduction

Indication that a kidney stone has fractured during shock wave lithotripsy (SWL) would aid a urologist in deciding to continue or cease treatment. Stopping treatment on a stone that is not breaking, and a good percentage of stones do not break, would potentially spare the patient acute injury and reduce the risk of chronic complications.[1,2] Our goal was to detect resonant scattering from kidney stone models to see if a stone fractured into two pieces could be distinguished from an intact stone. Resonant scattering is the term we use to describe the radiation caused by reverberations within a stone struck by a shock wave.

Although there is a vast field of techniques to detect calcifications in the body[3–6] and an equally large field of research on acoustic scattering,[7–9] clinical lithotripsy relies on B-mode ultrasound or fluoroscopy to target the stone. Little feedback is provided by these methods as to whether a stone has fractured. Generally, in the confines of the body to the resolution of the systems, it is difficult to distinguish an intact stone from a collection of stone fragments. Some research on feedback to target and track the stone has been completed. Thomas, Wu, and Fink[10] used time-reversal techniques in a peizoceramic lithotripter to target the stone. Borhis, Bayer, and Lechner[11] used spectral Doppler ultrasound to determine if a stone had been hit by a shock wave. Owen *et al.*[12] reported the use of vibro-acoustography to track the stone in water and thereby improved comminution. Chang *et al.*[13] developed a real-time tracking method to improve comminution, where analysis of ultrasound images was used to track the stone and to move the lithotripter accordingly. As for feedback on whether a stone has fractured, Fedele *et al.*[14] described a diagnostic sensor and signal processing technique, both under patent review, to assess the degree of stone fragmentation and stone location. The technique uses cavitation signals, where the secondary acoustic emission from bubble collapse is dependent on stone size.

Like Fedele *et al.*, we listen remotely with a broadband receiver during SWL, however our objective is to detect a difference in resonant scattering due to fractured stone pieces being

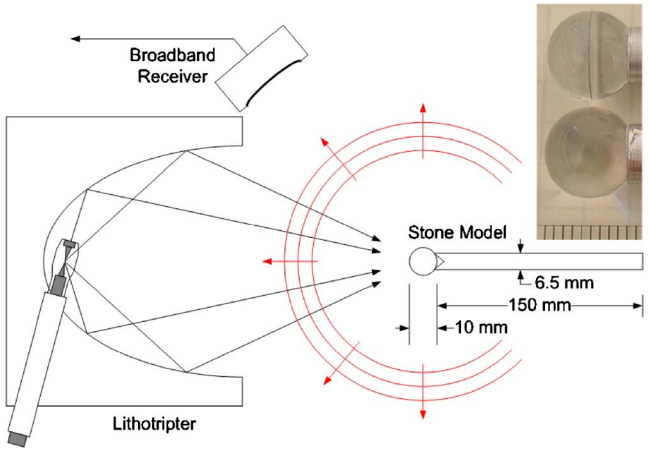

Fig. 1. (Color online) Illustration of the experiment for the calculation and measurement of acoustic scatter. The inset is a photograph of the intact and fractured stone models (marks on the scale are millimeters).

smaller than the intact stone. In this work, resonant scatter signals were calculated numerically and measured experimentally, and then compared to determine the scattering from stone models. A frequency analysis method was developed to distinguish between the intact and fractured stone models. During the *in vitro* experiments, high-speed photography was used to visualize cavitation.

2. Theory

Numerical simulation of the experiment (Fig. 1) was accomplished in three steps. First, a finite-difference time-domain numerical model for elastic wave propagation, developed originally to study stresses within kidney stones due to the impact of shock waves,[15] was used to calculate pressure in the liquid and stress in the stone model. An axisymmetric grid cast in cylindrical coordinates was initialized with a planar lithotripter shock pulse[16] with 40 MPa peak positive pressure, and with elastic coefficients (Table 1) representing the stone model and surrounding water. Results from this step were rendered into a movie (Mm. 1) to display the evolution of pressure and stress. Second, radiation from the stone model was calculated with the Helmholtz-Kirchhoff integral taken on a cylindrical surface surrounding the stone model.[17] The temporal wave form of acoustic pressure and its normal derivative in each grid point along this cylindrical surface was calculated during the first step. The Helmholtz-Kirchhoff integral allowed calculating the scattered pressure wave form at every point on the receiver. Third, the receiver signal was calculated by averaging acoustic pressure over a spherical bowl surface representing the focused receiver. Results from this final step were both compared to measurements of acoustic scatter and analyzed to determine fracture.

Mm. 1. Results from the linear elastic model that was used in the first step of calculation. Acoustic scatter comprises reflection and reverberation, which are most easily observed to the left of the stone models and along their axes (2.1 Mb). This is a file of type "mov".

Table 1. Elastic properties used in calculation (λ and μ are the Lamé constants)

	Sound speed m/s	Density kg/m^3	λ GPa	μ GPa
Glass	5600	2300	23.1	25
Epoxy	2720	1430	4.36	···
Aluminum	6300	2700	51.8	24
Water	1500	1000	···	···

3. Methods

In degassed water, intact and fractured stone models were placed individually at the focus of an electrohydraulic research lithotripter[18] and subjected to 20 shock waves. The experimental arrangement is illustrated in Fig. 1. Each shock wave was generated with a lithotripter charging potential of 17 kV, corresponding to 25 MPa peak positive pressure and 10 MPa peak negative pressure. The intact stone was modeled with a glass sphere of 5 mm radius that was bonded with epoxy to a counter-sunk aluminum rod for rigid placement in the acoustic field. Similarly, the fractured stone was modeled with two glass hemispheres of 5 mm radius that were bonded together with a 1 mm film of epoxy. A photograph of both models is shown in Fig. 1. Acoustic scatter from each shock wave was measured with a focused receiver, high-pass filtered at 100 kHz (Model 3202, Krohn-Hite Corporation, Brockton, MA), digitized at 50 MS/s (TDS744, Tektronix, Inc., Beaverton, OR) and saved in a computer. The filter was necessary to remove low frequency noise, presumably a combination of a structural resonance of the receiver and transient electrical signals from the high voltage discharge.

The remote broadband receiver was designed to measure acoustic scatter without blocking the acoustic path between the lithotripter and the stone models (Fig. 1). It was fabricated with a polyvinylidene fluoride (PVDF) film of 25 μm thickness and 50 mm diameter that was formed to a spherical curvature with a radius of 150 mm. With the addition of a differential amplifier, the −3 dB pass band was between 100 kHz and 10 MHz. The receiver was fabricated at the Center for Industrial and Medical Ultrasound as an extension of recent literature.[19] Focal properties were characterized by wiring the PVDF film as a source, exciting it at 3.6 MHz, and measuring the resulting acoustic field with a hydrophone (GL-0150-1A, Specialty Engineering Acoustics, Soquel, CA). The axial and lateral dimensions of the pressure focus measured at −6 dB were 45 and 2 mm, respectively.

Effort was made to reduce cavitation in the experiments. Stone models were made of smooth, lens quality glass, because glass wets and adheres well to water. The lithotripter was operated at a low charging voltage of 17 kV to reduce the negative pressure of the shock wave. Each shock wave was triggered 1 min apart to allow bubbles to dissolve.[20] Last, digital photography was used to visualize cavitation. A high-speed camera (Imacon 200, DRS Technologies, Parsippany, NJ), 105 mm lens, and 27.5 mm extender produced a 2.0 cm × 2.4 cm field of view in 980 × 1200 pixels.

Calculated and measured signals were processed using MATLAB (The Mathworks, Inc., Natick, MA). Measured signals were deconvolved with a sampled approximation of the high-pass filter's impulse response. Deconvolution removed the transient effects of the filter but also added high frequency noise, caused in part by division in frequency, which was removed with a 10 MHz low-pass filter. Twenty measured wave forms were then aligned in time to correct for jitter in the shock wave trigger timing, and then averaged. Averaging was intended to compensate for shot-to-shot variation in the shock pulse, but had little effect on the signals since they were quite repeatable. Time domain processing was not performed on signals obtained from calculation.

Several steps were used to analyze calculated and measured data in the frequency domain. First, specular reflection of the shock wave, a sequence lasting about 5 μs, was found to be similar for data from both the intact and fractured stone models. To isolate the differences in wave forms from the two models, the sequence of specular reflection was truncated and 15 μs of resonant scattering, resulting from reverberation in the stone and directly following the specular reflection, was retained. Second, to compare the data based on frequency alone, each sequence was normalized by its root-mean-square value. Third, the power spectral density of each sequence was found. Fourth, energy values, E, were calculated, based on Parseval's theorem, by integrating the power spectra over two distinct bands in frequency, from $f_1 = 0$ to $f_2 = 0.5$ MHz and from $f_1 = 0.5$ MHz to $f_2 = 2.0$ MHz

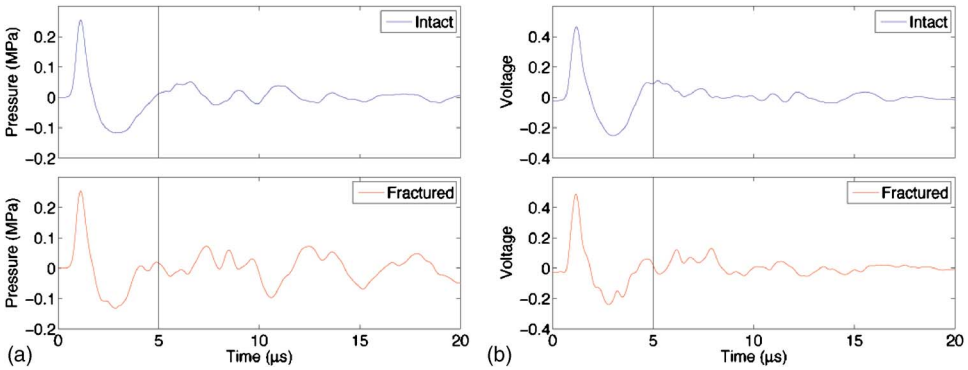

Fig. 2. (Color online) Acoustic scatter from (a) calculation and (b) measurement. The vertical line at 5 μs roughly separates the segments of reflection of the shock wave and resonant scattering caused by reverberation. Segments of reflection (left of the vertical line) were truncated and segments of reverberation (right of the vertical line) were retained for analysis in the frequency domain. Since the PVDF receiver was not calibrated, the amplitude of measured signals are presented in volts.

$$E = \sum_{k=f_1/\Delta f}^{f_2/\Delta f} W_k \cdot \Delta f, \tag{1}$$

where W_k is the discrete power spectral density sequence at frequency $f=k\Delta f$, k is an index variable, f_1 and f_2 are end points of the aforementioned frequency bands, and Δf is the difference between adjacent samples in frequency. Last, in each frequency band a ratio was found by

$$R = \frac{E_F}{E_I}, \tag{2}$$

where R is the ratio of energies, E_F is energy calculated with Eq. (1) using data from the fractured stone model, and E_I is energy calculated with Eq. (1) using data from the intact stone model. A ratio using Eq. (2) was found separately for both calculated and measured data. The expectation was that resonant scattering from the fractured stone model would be characterized by higher frequencies, therefore the ratio of energies is meant to distinguish between the two stone models.

4. Results

Mm. 1 shows calculated acoustic scattering from the two stone models. Glass spheres and hemispheres are traced in black and the aluminum rods are traced in white; all other colors represent a stress or pressure value. Upon impingement, the shock wave is both reflected by the surface of the stone models and transmitted into the stone models. A clear difference in the scattered field is visible when the movie is paused at $t=15$ μs. At that time, to the left of the stone models and along their axes, the reflected shock waves are followed by pressure fluctuations in the water that correspond to reverberations within the stone models. These reverberations represent nothing other than vibrational resonance of the stone after excitation by a broadband load associated with a short lithotripter pulse. The result can therefore be called resonant scattering. As is always the case for vibration of an elastic object, the resonance frequency is inversely proportional to the object size. Compared to the intact stone model, pressure fluctuations emitted by the fractured stone model are closer together and of higher amplitude. This effect is caused by the glass hemispheres being smaller than the glass sphere and by the strong reflection at the planar surfaces between the hemispheres. The difference is less off axis.

Measured and calculated wave forms from intact and fractured stone models are shown in Fig. 2. The vertical lines separate the sequences of reflection, to the left, and resonant scattering, to the right. Results generally agree well when comparing calculation and measure-

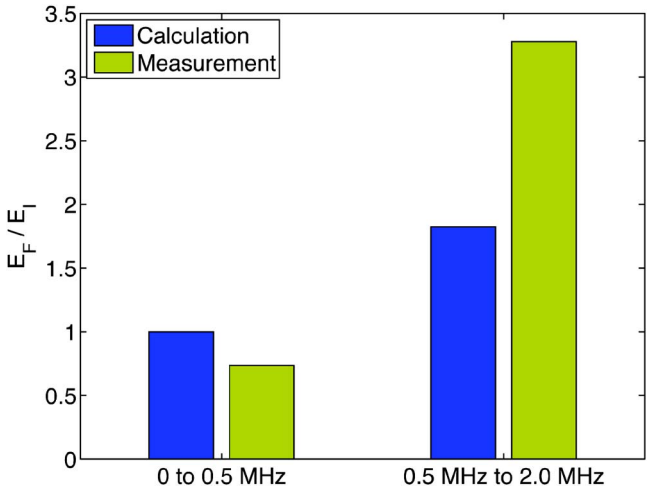

Fig. 3. (Color online) The ratio of energies between fractured and intact stones, $R=E_F/E_I$, in frequency bands for signals from calculation and measurement. Both calculation and measurement show increased energy in the frequency band between 0.5 and 2.0 MHz, which indicates that the intact and fractured stone models can be distinguished.

ment, especially the reflection of the shock wave between times 0 and 5 μs. Wave forms from intact and fractured stone models have noticeable differences. For the intact stone model, one reverberation across the axial diameter of the sphere is 3.6 μs using a sound speed of 5600 m/s (Table 1). Accordingly, pressure fluctuations corresponding to waves within the stone model begin approximately 3.6 μs after the peak positive pressure of the reflected shock wave. Similarly for the fractured stone model, pressure fluctuations begin sooner, at 1.8 μs after the peak positive pressure of the shock wave, and are of higher amplitude. The respective periods of resonant acoustic scatter, 3.6 and 1.8 μs, are evident.

Figure 3 shows the ratios, $R=E_F/E_I$ (see Eq. (2)), found with frequency-domain processing for calculated and measured results. The frequency bands were chosen based on reverberation times for the stone models, where a period of 3.6 μs corresponds to 280 kHz and a period of 1.8 μs corresponds to 560 kHz. Both calculation and measurement show increased energy in the frequency band between 0.5 and 2.0 MHz, indicating that the fractured stone model can be distinguished from the intact stone model.

Figure 4 shows high-speed images of the intact stone model taken simultaneously with acoustic scattering detection. In the photographs, there are no bubbles visible before the shock wave arrives at 0 μs and only tiny bubbles growing at 26 μs, which is after our data have been recorded. The signal below the photographs is the scattering signal recorded not only for the first 20 μs, as in Fig. 2, but for hundreds of microseconds following shock wave arrival. Together the photographs and signal indicated that little noise was received as the bubbles grew and a detectable pressure spike was generated when the bubbles collapsed and rebounded at about 250 and 350 μs. Photographic and recorded results from the fractured stone model were similar.

5. Discusssions and conclusions

Calculated and measured scattering from an intact stone model and a model with a fracture normal to the shock wave axis agree well in the time domain. We speculate minor discrepancies are primarily due to neglecting shear waves in the epoxy in the model; an exact value for the Lamé constant, μ, was not known. Both calculation and measurement show the fractured stone reverberated at a higher frequency and that fractured stones could be distinguished from intact

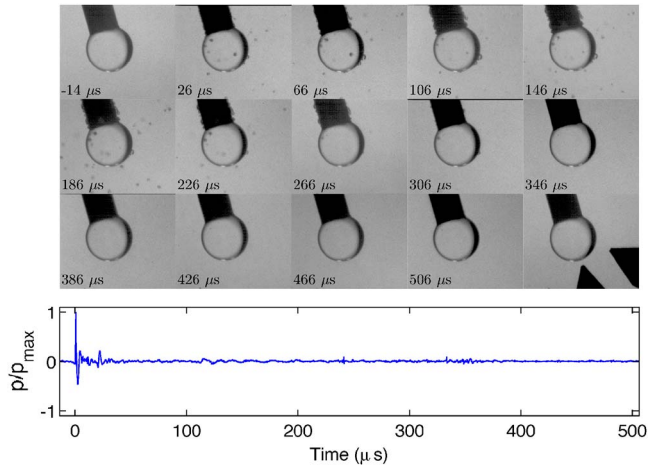

Fig. 4. (Color online) High-speed photography of the intact stone model subjected to a single shock wave and the corresponding measured acoustic scatter wave form. Each photograph is 2.0 cm × 2.4 cm and labeled with a time relative to $t=0$ μs, when the shock wave arrived at the stone. The bottom right photograph illustrates with black pointers the axes of the shock wave (bottom) and the receiver (right). Below the photographs is the measured wave form, where the propagation time between the stone and the receiver has been subtracted. The period of acoustic scatter used for analysis is between times 0 and 20 μs. Bubble collapse and rebound events generally happen much later, at about 250 and 350 μs here, and do not influence the period of resonant scatter.

stones. A method using the ratio of energies in distinct bands, related to stone size, was developed to clearly and simply display the difference between the intact and fractured stone models.

This work was a carefully controlled *in vitro* study, and although clearly obstacles exist, many results are encouraging for further *in vivo* study. Cavitation may occur *in vivo*, and its effect on the signals is not known. However, it was possible to avoid disruption of the measured signals, as evidenced by good agreement with the model which does not account for cavitation, by making an effort to reduce cavitation such as giving bubbles time to dissipate before taking measurements. Real kidney stones can have irregular nonspherical shape, but the dominant effects observed here, which were used to identify fracture, are related to the reverberation time across the length of the stone. Scatter measured remotely from stones *in vivo* may have lower amplitude than glass stones in water, but the signals obtained here are very strong, hundreds of millivolts, so some attenuation or reduction in signal amplitude might be tolerated. Measured signals were intentionally shown as voltage to show this amplitude. For pressure amplitudes, the receiver could be calibrated by comparing the scattered signals to measurements taken with a hydrophone at the location of the scatterer. The calibrated system can then be used to measure high intensity ultrasound fields without damage to a hydrophone.[21,22]

The geometry of the counter-sunk aluminum rods may have affected the experiment by increasing the scattering amplitude over another arrangement. They were meant to hold the model stones rigidly in order to study shot to shot variability in the receive signal and to facilitate averaging, which, for example, would remove random noise from cavitation. However, results indicate the measurement was repeatable and that cavitation was not the dominant effect. Choosing the counter-sunk end was also influenced by the numerical experiment, which was axisymmetric, and intended for the surface area of contact between the glass, epoxy, and rod to be consistent for both model stones. Any effect in frequency caused by the rods would have been the same for both model stones, and therefore would not influence the ratio of energies used to distinguish the model stones. Also, a long length was chosen for the rod to prevent reflection from the distal end from contaminating the measurement. Work in progress involves measuring acoustic scatter from breakable model stones held within a plastic pipette, which allows the stones to move.

The study here looked at resonant acoustic scatter as feedback to identify fracture; however, because the technique essentially detects a change in frequency related to the change in size of the stone, our technique lays the groundwork for assessment of complete comminution. Potentially this concept could be used to determine if fragments are sufficiently small to pass from the body and thus that treatment is completed.

Acknowledgments

The authors thank Brian MacConaghy and Adam Maxwell for design and fabrication of the spherical receiver; the investigators, staff, and students at the Center for Industrial and Medical Ultrasound; and the Consortium for Shock Waves in Medicine. This work was supported by: NIH DK43881, DK55674, NSBRI SMS00402, and RFBR 05-02-16987.

References and links

[1]J. E. Lingeman and J. R. Newmark, "Adverse bioeffects of shock-wave lithotripsy," in *Kidney Stones: Medical and Surgical Management*, edited by F. L. Coe *et al.* (Lippencott-Raven, Philidelphia, 1996), pp. 605–614.
[2]A. P. Evan, A. R. Willis, J. E. Lingeman, and J. A. McAteer, "Renal trauma and the risk of long-term complications in shock wave lithotripsy," Nephron **78**, 1–8 (1998).
[3]P. N. Rao, "Imaging for kidney stones," World J. Urol. **22**, 323–327 (2004).
[4]L. Gao, K. J. Parker, R. M. Lerner, and S. F. Levinson, "Imaging of the elastic properties of tissue—A review," Ultrasound Med. Biol. **22**, 959–977 (1996).
[5]M. Fatemi and J. F. Greenleaf, "Ultrasound-stimulated vibro-acoustic spectrography," Science **280**, 82–85 (1998).
[6]K. Nightingale, M. S. Soo, R. Nightingale, and G. Trahey, "Acoustic radiation force impulse imaging: In vivo demonstration of clinical feasibility," Ultrasound Med. Biol. **28**, 227–235 (2002).
[7]A. D. Pierce, *Acoustics: An Introduction to its Physical Principles and Applications* (Acoustical Society of America, New York, 1991).
[8]A. Ishimaru, *Wave Propagation and Scattering in Random Media* (IEEE, Piscataway, NJ, 1997).
[9]P. M. Morse, *Vibration and Sound* (Acoustical Society of America, New York, 1981).
[10]J. L. Thomas, F. Wu, and M. Fink, "Time reversal focusing applied to lithotripsy," Ultrason. Imaging **18**, 106–121 (1996).
[11]C. Bohris, T. Bayer, and C. Lechner, "Hit/miss monitoring of ESWL by spectral Doppler ultrasound," Ultrasound Med. Biol. **5**, 705–712 (2003).
[12]N. R. Owen, M. R. Bailey, A. Maxwell, B. MacConaghy, T. D. Khokhlova, and L. A. Crum, "Vibro-acoustography for targeting kidney stones during lithotripsy," J. Acoust. Soc. Am. **116**, 2509 (2004).
[13]C. C. Chang, I. Manousakas, Y. R. Pu, M. Liang, C. H. Chen, F. M. Yu, W. H. Yang, Y. C. Tong, and C. L. Kuo, "In vitro study of ultrasound based real-time tracking for renal stones in shock wave lithotripsy: Part II—A simulated animal experiement," J. Urol. (Baltimore) **6**, 2594–2957 (2002).
[14]F. Fedele, A. J. Coleman, T. G. Leighton, P. R. White, and A. M. Hurrell, "Development of a new diagnostic sensor for extra-corporeal shock-wave lithotripsy," in *Proceedings of the First Mediterranean Conference on Medical and Biological Engineering*, "Health in the Information Society," pp. 134–139, (Naples, Italy, 2004).
[15]R. O. Cleveland and O. A. Sapozhnikov, "Modeling elastic wave propagation in kidney stones with application to shock wave lithotripsy," J. Acoust. Soc. Am. **118**, 2667–2676 (2005).
[16]C. C. Church, "A theoretical study of cavitation generated by an extracorporeal shock wave lithotripter," J. Acoust. Soc. Am. **86**, 215–227 (1989).
[17]O. A. Sapozhnikov, L. A. Trusov, N. R. Owen, M. R. Bailey, and R. O. Cleveland, "Detecting fragmentation in kidney stones in lithotripsy by means of shock wave scattering," in *Fifth International Symposium on Therapeutic Ultrasound*, edited by G. T. Clement, N. J. McDonald, and K. Hynynen (American Institute of Physics, New York, 2005), pp. 308–312.
[18]R. O. Cleveland, M. R. Bailey, N. Fineberg, B. Hartenbaum, M. Lokhandwalla, J. A. McAteer, and B. Sturtevant, "Design and characterization of a research electrohydraulic lithotripter patterned after the Dornier HM3," J. Acoust. Soc. Am. **71**, 2514–2525 (2000).
[19]J. A. Ketterling, O. Aristiżabal, D. H. Turnbull, F. L. Lizzi, "Design and fabrication of a 40 MHz annular array transducer," IEEE Trans. Ultrason. Ferroelectr. Freq. Control **52**, 672–681 (2005).
[20]T. G. Leighton, *The Acoustic Bubble* (Academic, London, 1994).
[21]P. Kaczkowski, B. Cunitz, V. Khokhlova, and O. A. Sapozhnikov, "High resolution mapping of nonlinear MHz ultrasonic fields using a scanned scatterer," in *IEEE Ultrasonics Symposium* (Honolulu, Hawaii2003), pp. 982–985.
[22]M. E. Schafer, J. Gessert, and W. Moore, "Development of a high intensity focused ultrasound (HIFU) hydrophone system," in *Fifth International Symposium on Therapeutic Ultrasound*, edited by G. T. Clement, N. J. McDonald, and K. Hynynen (American Institute of Physics, New York, 2005), pp. 609–613.

